

## PAPER

# Respiratory Motion and Correction Simulation Platform for Coronary MR Angiography

Florencio Rusty PUNZALAN<sup>†a)</sup>, *Nonmember*, Tetsuo SATO<sup>†</sup>, *Member*, Tomohisa OKADA<sup>††</sup>, Shigehide KUHARA<sup>†††</sup>, Kaori TOGASHI<sup>††</sup>, *Nonmembers*, and Kotaro MINATO<sup>†</sup>, *Member*

**SUMMARY** This paper describes a simulation platform for use in the quantitative assessment of different respiratory motion correction techniques in Coronary MR angiography (CMRA). The simulator incorporates acquisition of motion parameters from heart motion tracking and applies it to a deformable heart model. To simulate respiratory motion, a high-resolution 3-D coronary heart reference image is deformed using the estimated linear transformation from a series of volunteer coronal scout scans. The deformed and motion-affected 3-D coronary images are used to generate segmented  $k$ -space data to represent MR data acquisition affected by respiratory motion. The acquired  $k$ -space data are then corrected using different respiratory motion correction methods and converted back to image data. The resulting images are quantitatively compared with each other using image-quality measures. Simulation experiment results are validated by acquiring CMRA scans using the correction methods used in the simulation.

**key words:** *respiratory motion, MRI simulation, simulation platform, coronary MR angiography*

## 1. Introduction

Coronary Magnetic Resonance Angiography (CMRA) has been increasingly used in the clinical imaging of coronary arteries. It offers sharp contrast between the blood and the arterial wall and enables a more accurate diagnostic of lesions and arterial blockage. Since it is a form of magnetic resonance imaging (MRI), it does not expose patients to radiation, unlike computed tomography (CT) or positron emission tomography (PET). However, CMRA can be adversely affected by patient motion, more specifically by cardiac cycle and respiratory motion. Cardiac cycle motion is usually addressed using electrocardiography (ECG) triggering [1].

Many studies have been done to compensate for respiratory motion and avoid image degradation in CMRA. The more common methods are under the *prospective* motion correction type, which predict and correct for respiratory motion during the duration of the scan. These include the navigator-guided, one-dimensional (1-D) translation correction [2]. This method tracks the motion of the diaphragm

in the superior-inferior (SI) direction and uses a fixed multiplier to approximate the motion of the heart. This multiplier, which is usually called the *correction factor (CF)* and has a standard value of 0.6, indicates the movement of the heart, in mm, for every 1 mm movement of the diaphragm. The method is commonly used in CMRA scanners because it is simple and easy to implement. However, it treats the heart as a rigid object and does not entirely describe the respiratory heart motion. Other more recent studies try to correct for two- and three-dimensional motion [3], [4]. The increase in motion approximation accuracy consequently increases the complexity of implementing the method in the MR scanner. More complex methods are not easily implemented in scanners because of their proprietary nature. In addition, the more complex the correction becomes, the more it can add to the possibility of prolonging CMRA scans, which already take around 20 to 30 minutes for each patient.

In addition, the acquisition of a high quality 3-D coronary data depends on the patient or subject under study. The respiratory motion of the heart is highly subject-specific [5]. This presents a problem during acquisition since the tailoring of correction for each patient can add to acquisition time. It adds a factor for CMRA clinicians and radiologists to consider in deciding which is the appropriate and practical correction method for them.

The number of these respiratory motion studies and complexity of their implementation makes it impractical to test and evaluate them for multiple subjects. A quantitative comparison of these proposed methods is also not available because these studies used different types of scanners and different subjects. To clinically evaluate these methods using the same scanner and subjects would be impractical and time-consuming. Furthermore, the use of clinical scans would result in other sources of artifacts affecting the image quality of the resulting scan like cardiac cycle motion and magnetic inhomogeneities in the machine [6]. A quantitative comparison should be able to measure the effectiveness of a motion correction study while eliminating the effects of other sources of motion. With this, we propose a method to quantitatively compare different respiratory motion correction techniques, independent of other sources of motion and image artifacts.

We designed and implemented a CMRA simulation platform that clinicians can use to compare different respiratory motion correction methods. The simulation software can run in general purpose computers, so the clinicians does

Manuscript received March 13, 2012.

Manuscript revised August 10, 2012.

<sup>†</sup>The authors are with School of Information Science, NAIST, Ikoma-shi, 630-0192 Japan.

<sup>††</sup>The authors are with Kyoto University Hospital, Kyoto-shi, 606-8507 Japan.

<sup>†††</sup>The author is with Toshiba Medical Systems, Otawara-shi, 324-8550 Japan.

a) E-mail: floren@ritsumeai.ac.jp

DOI: 10.1587/transinf.E96.D.111

not have to implement the different methods under evaluation in the actual scanner. In addition, it can be used to standardize the evaluation of correction methods. The platform utilizes a patient-based voxelized model with the capacity to recreate the patient-specific respiratory motion derived from cardiac MR scout scans.

In terms of using the navigator-guided 1-D translation correction, we used the platform to evaluate different  $CF$  candidates to determine which  $CF$  can best predict a subject's respiratory motion. We evaluated this method because it is readily available in most clinical scanners, including the one we used in this study.

## 2. Method

The proposed simulation platform for comparing respiratory motion correction methods is composed of two major parts, namely, respiratory motion model and CMRA motion correction simulator. The respiratory motion model recreates the subject-specific cardiac motion as a function of diaphragm motion. The respiratory motion modelling involves tracking and correlating the diaphragm and heart motion from real 2-D scout scans. The CMRA motion simulator virtually implements motion correction methods to correct the simulated respiratory-induced motion artifacts on a CMRA scan. The simulation method uses the  $k$ -space formalism to introduce and correct motion in a reference 3-D scan. In addition, the motion correction simulator includes the quantitative image quality comparison of the generated scans from different correction methods.

### 2.1 Simulation Platform Algorithm

This section describes the inputs and outputs of the proposed simulation platform as well as the steps to generate the outputs. Given a set of 2-D MRI scout scans  $\mathbf{R} = \{R_1, R_2, \dots, R_M\}$ , where  $M$  is number of 2-D image slices, and a reference 3-D Coronary MRA image  $\mathbf{Q}_{Ref}$ , the goal of the simulation platform is to find the motion correction method  $c_p$  from  $C = (c_1, c_2, \dots, c_Z)$  that can best predict the respiratory-induced motion of the heart during the CMRA scan. The simulation platform process can be described with the following algorithm:

1. Estimate the respiratory motion correlation coefficients from a set of 2-D MRI scout scans.
2. Generate a discrete respiratory waveform with  $K$  translation levels from a randomly-generated sinusoidal wave.
3. Apply spatial transformation to a reference 3-D Coronary MRA image,  $\mathbf{Q}_{Ref}$ , for each translation level  $y_k \in Y = \{y_1, y_2, \dots, y_K\}$  using the estimated correlation coefficients.
4. Acquire the uncorrected  $k$ -space data,  $\mathbf{Q}_{nc}$ , using *in-vivo* MRI  $k$ -space acquisition simulation and by sampling the respiratory waveform.
5. Apply motion correction to the uncorrected  $k$ -space

data  $\mathbf{Q}_{nc}$  for each of the correction methods in  $C = (c_1, c_2, \dots, c_Z)$ .

6. Transform all the motion-corrected  $k$ -space data into 3-D CMRA image data.
7. Assess the effectiveness of each method in  $C$  by comparing the resulting 3-D CMRA images using some commonly-used image quality measures.

Steps 1–3 of the algorithm above belong to the respiratory motion model part, while steps 4–7 belong to the CMRA motion simulator part.

As an example implementation of the proposed system, we used the comparison of using different values of the correction factor in respiratory motion correction. It assumes that a single  $CF$  is used to correct for respiratory motion during CMRA scan, which is the technique commonly utilized in many scanners today. The values of  $CF$  are estimated from the *correlation coefficient* ( $CC$ ) values between the diaphragm and heart motion. These values are derived from the set of time-series 2-D coronal scout scans  $\mathbf{R}$ . The final product of the simulation is the correction factor  $CF = c_p$  which gives the 3-D data with the highest image quality in terms of SNR, CNR, vessel length and vessel edge definition.

The following subsections give a more detailed description of the steps in the algorithm. Section 2.2.1 elaborates on how the  $CC$ s are estimated. Sections 2.2.2 and 2.2.3 describe how the respiratory waveform is generated and the reference scan is transformed, respectively. In addition, the last part of the Method section details the motion correction simulator, which includes the simulation of MR  $k$ -space data acquisition and motion correction.

### 2.2 Respiratory Motion Model

#### 2.2.1 Motion Parameter Estimation

The first step in simulating respiratory motion correction is to model the subject-specific respiratory-induced motion of the heart. This involved tracking the heart as it moves with the diaphragm during respiration and measuring its correlation coefficients. The tracking was done on a cine scout scan, which is a two-dimensional, time-series image data showing the heart in the coronal plane. In order to get the  $CC$  values of the heart, six regions of interest (ROI) were tracked for each image in the cine scan. Diaphragm motion was tracked using a rectangular ROI with dimensions of  $30 \times 10$  pixel, placed in the dome of right hemidiaphragm (Fig. 1). The remaining ROIs were placed along the edges of the heart to track the superior-inferior (SI) and right-left (RL) cardiac motion. To measure the displacement, the SI location of the horizontal edge was subtracted from a fixed reference location. The edge location is detected by computing for the gradient magnitude of each horizontal line in the ROI and then searching for the local maxima of the gradient.

Least-squares method was used to determine the edge

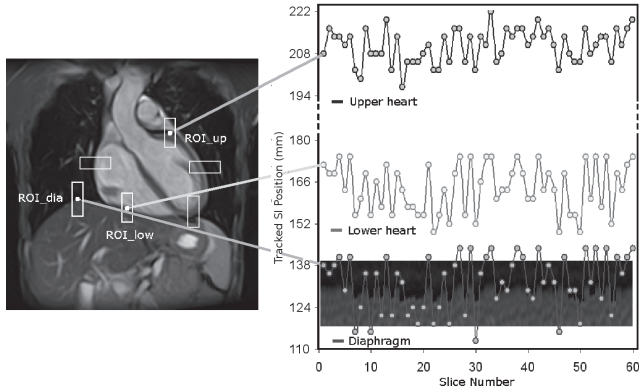


**Fig. 1** Region-of-interest (ROI) motion tracking model for the diaphragm and heart. The right side shows the tracked location of the diaphragm and the heart ROI for all images in the scout scan. The tracked locations are used to compute the correlation coefficient ( $CC$ ) values.

---

### Algorithm 1.1: Estimation of motion parameters.

---

**Data:**  $R = \{R_1, R_2, \dots, R_M\}$ .

**Result:** correlation coefficient  $CC_{upr}$  and  $CC_{lwr}$ .

**for**  $m \leftarrow 1$  **to**  $M$  **do**

  place regions of interest (ROIs) in  $R_i$   
    $diaph\_loc[m] \leftarrow \text{measureDiaphragmLocation}(R_m)$   
    $heUpr\_loc[m] \leftarrow \text{measureUpperHeartLocation}(R_m)$   
    $heLwr\_loc[m] \leftarrow \text{measureLowerHeartLocation}(R_m)$

$CC_{upr} \leftarrow \text{calcCorrelCoef}(diaph\_loc, heUpr\_loc)$

$CC_{lwr} \leftarrow \text{calcCorrelCoef}(diaph\_loc, heLwr\_loc)$

$C \leftarrow \text{assignCorrectionFactors}(CC_{upr}, CC_{lwr})$

---

displacements inside the ROIs. The measured displacements for each image are then correlated with the corresponding displacements of the diaphragm. The slope of the linear regression lines in the correlation graph (*i.e.* diaphragm vs. heart ROI) was assigned as the  $CC$  value for that region of the heart. The  $CC$  estimation part of the algorithm (Step 1) for the upper ( $CC_{upr}$ ) and lower ( $CC_{lwr}$ ) heart can be summarized as shown in Algorithm 1.1.

### 2.2.2 Respiratory Waveform Generation

To simulate the rhythmic motion of the diaphragm during tidal breathing, we created an arbitrary sinusoidal waveform with a randomly varying frequency. The frequency range was set at 0.33 to 0.2 Hz to reflect the average range of respiratory rate for adults, which is around 12 to 20 breaths per minute. We used a sinusoidal wave so that we can easily randomize the frequency of respiration. Consequently, a real data of diaphragm motion (*e.g.* from respiratory bellows) can also be used to provide a more realistic waveform shape and frequency variation. The generated diaphragm waveform is described by the following continuous equation:

$$diaph(t) = 0.5 \cos\left(\frac{\pi}{P_r}t\right) + 0.5 \text{ cm},$$

---

### Algorithm 1.2: Generation of the discrete respiratory waveform.

---

**Data:** diaphragm trans levels  $Y = \{y_1, y_2, \dots, y_K\}$ .

**Result:** discrete respiratory waveform  $diaph[]$ .

generate continuous respiratory waveform  $diaph(t)$

assign  $N$  as number of discrete samples

**for**  $n \leftarrow 1$  **to**  $N$  seconds **do**

$[diaph[n]] \leftarrow \text{sampleResWave}(n, diaph(t))$ , where  $diaph[n] \in Y$

---

$$0.20 \leq \frac{1}{P_r} \leq 0.33 \text{ Hz}, \quad (1)$$

where  $P_r$  denotes the random respiration period (3–5 s) and  $t$  is the time in seconds. The waveform oscillates in the  $[0, 1]$  amplitude range, which is set as the displacement range of the diaphragm from end-expiration to end-inspiration (in cm). The amplitude range is divided into  $K$  discrete levels or positions with each level having the value of  $y_k$ , where  $k = 1$  to  $K$ . The amplitude of 1 cm is the default maximum displacement of the diaphragm in the simulation platform but this can easily be changed into any value, depending on the measured diaphragm movement of the subject. The discrete respiratory waveform generation procedure (Step 2) can be summarized in Algorithm 1.2.

### 2.2.3 Spatial Transformation of Reference Image

The estimated correlation coefficients from the scout scans are used to model the movement and deformation of the heart with respect to respiration. Even though most of the motion of the heart is SI translation, SI scaling and RL translation and scaling were also included. A 2-D affine transformation matrix was used to transform each 2-D slice in the 3-D image using the following equation:

$$T = Ar + v = \begin{pmatrix} s_x \cos\theta & -s_y \sin\theta \\ s_x \sin\theta & s_y \cos\theta \end{pmatrix} \begin{pmatrix} x \\ y \end{pmatrix} + \begin{pmatrix} d_x \\ d_y \end{pmatrix}, \quad (2)$$

where  $A$  is the linear transformation,  $r$  is the Cartesian coordinate and  $v$  is the translation vector. The variables  $s_x$ ,  $s_y$  and  $d_x$ ,  $d_y$  are the scaling and translation parameters in the  $x$  and  $y$  direction, respectively, while  $\theta$  is the corresponding rotation angle.

The translation parameter  $d_y$  is derived from the average between the motion coefficients of the upper and lower heart. Given the correlation coefficient for the upper ( $CC_{upr}$ ) and lower right ( $CC_{lwr}$ ) part of the heart, the translation parameter in the SI direction is

$$d_y = \frac{CC_{lwr} + CC_{upr}}{2}. \quad (3)$$

The scaling factor  $s_y$  is computed such that it reflects the difference between the upper and lower heart motion. The value is normalized across the height of the heart, as shown by the equation

$$s_y = 1 + \frac{CC_{lwr} + CC_{upr}}{|r_{2y} - r_{5y}|}, \quad (4)$$

---

**Algorithm 1.3:** Transformation of the reference image for every translation level  $y_k$ .
 

---

**Data:** high-quality 3-D CMRA reference scan  $Q_{Ref}$  and correlation coefficients  $CC_{upr}$  and  $CC_{lwr}$ .

**Result:** transformed dataset  $Q[]$ .

```

 $A(s_x, s_y) \leftarrow \text{calcScalingParams}(CC_{upr}, CC_{lwr})$ 
 $v(d_x, d_y) \leftarrow \text{calcTranslationParams}(CC_{upr}, CC_{lwr})$ 
for  $k \leftarrow 1$  to  $K$  do
   $T_k \leftarrow \text{createTransformMatrix}(y_k, A, v)$ 
   $Q[k] \leftarrow \text{applyTransformation}(Q_{Ref}, T_k)$ 
  
```

---

where  $|r_{2y} - r_{5y}|$  corresponds to the SI distance between the edge of the lower right and upper heart (*i.e.* height of the heart). The translation and scaling parameters used in the simulation were based from the upper and lower heart coefficients gathered in the first part of this study with additional coefficients added as arbitrary values.

To simulate heart displacement during respiration, the reference dataset is first assigned as an undeformed heart located in end-expiration. The simulated diaphragm motion range is set to the default value of 10 mm, from end-expiration to end-inspiration. The spatial resolution of the diaphragm movement is 0.5 mm, which gives a total of 20 diaphragm positions ( $y_1, y_2, \dots, y_{20}$ ) for the whole range of motion, excluding the end-expiration position. For each level  $y_k$ , the reference image  $Q_{Ref}$  undergoes spatial transformation to generate the transformed 3-D image  $Q[k]$ . The transformation is done by multiplying each voxel in the reference image by the transformation matrix  $T_k$ . The process of generating the transformed images for each diaphragm translation level (Step 3) can be summarized in Algorithm 1.3.

## 2.3 CMRA Motion Correction Simulator

### 2.3.1 Acquisition of Uncorrected $k$ -Space Data

After each transformation, the the transformed 3-D image  $Q[k]$  is converted to  $k$ -space data  $Q[k]$  using 3-D Fast Fourier Transform (FFT). Each of these data in the  $k$ -space dataset is used for simulating the MR acquisition of the uncorrected data  $Q_{nc}$ .

MR image acquisition involves the filling of  $k$ -space data. The  $k$ -space represents the spatial frequency information in two or three dimensions of an object. In an actual MRI scanner, the phase and frequency encoding data is structured in this  $k$ -space grid, which is filled one line (or multiple lines) at a time until the image is complete.

The  $k$ -space data is in Fourier space and contains all the necessary information to reconstruct an image. It is related to the image data through the Fourier transformation. Sampling of the acquired signal in MRI is arranged such that low-frequency signals are at the center of the acquired data and the high-frequency signals are placed around this center. The rightmost column of Fig. 2 shows examples of a typical uniformly sampled  $k$ -space data.

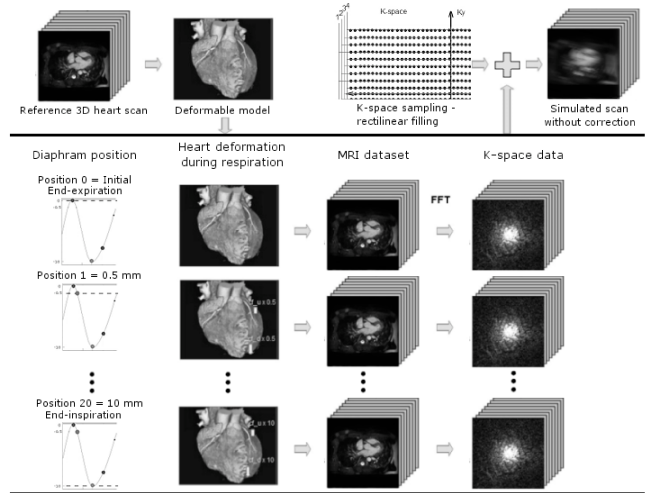


**Fig. 2** Method for generating the  $k$ -space dataset of the deformed cardiac model for each respiratory diaphragm position. The range of the respiratory waveform is divided into  $k$  discrete levels or positions and in each level a transformed reference image is produced. The transformed 3-D images are then converted to  $k$ -space data using FFT. The generated  $k$ -space data for each diaphragm displacement level are used to create the simulated CMRA acquisitions.

---

**Algorithm 1.4:** Acquisition of Uncorrected 3-D  $k$ -space.
 

---

**Data:** transformed dataset  $Q[]$  and discrete resp waveform  $diaph[]$ .

**Result:** uncorrected 3-D  $k$ -space data  $Q_{nc}$ .

```

for  $k \leftarrow 1$  to  $K$  do
   $Q[k] \leftarrow \text{imageToKspace}(Q[k])$ 
 $Q_{nc} \leftarrow \text{sampleKspaceData}(Q, diaph[])$ 
  
```

---

To acquire MRI data in the simulation platform,  $k$ -space data acquisition is performed during each sampled point in the generated respiratory waveform  $diaph(t)$ . Figure 2 shows that a  $k$ -space equivalent  $Q[k]$  is acquired for each transformed image  $Q[k]$ . Each point in the sampled waveform corresponds to a diaphragm position where the  $k$ -space line(s) will be acquired. The procedure mimics an *interleaved* acquisition in actual MRI, where a set of  $k$ -space lines is acquired in one cardiac cycle using segmented rectilinear encoding. A complete dataset is created when all the  $k$ -space lines in the volume are filled. The acquisition of the 3-D  $k$ -space data without motion correction (Step 4) can be summarized in Algorithm 1.4.

### 2.3.2 Motion Correction Simulation

Once the uncorrected  $k$ -space data is generated, a motion correction can be applied using a correction method and the data on diaphragm displacement positions used to acquire the uncorrected data.

The platform was used to compare the effect of different correction factors on the image quality of the resulting simulated scans. First, the motion coefficients to be used

for the simulations were measured for one of the volunteer scans. A pair of motion coefficients of 0.46 and 0.56 for the upper and lower heart, respectively, were used for the simulations. Once the motion coefficients were determined, five different CMRA simulations were generated. A 3-D volume data was acquired for each of the following methods:

1. Acquisition without motion compensation ( $Q_{nc}$ ).
2. Using the standard correction factor ( $CF = 0.6$ ).
3. Using  $CC_{upr}$  as correction factor ( $CF_{upr}$ ).
4. Using  $CC_{lwr}$  as correction factor ( $CF_{lwr}$ ).
5. Using the mean correction factor ( $CF_{mean}$ ), the average of  $CF_{upr}$  and  $CF_{lwr}$ .

To complete the simulation, the 3-D images were reconstructed from the  $k$ -space data using inverse-FFT. Lastly, each 3-D image was evaluated and compared to the original scan using a number of image-quality measures.

### 3. Experiments

To measure the correlation coefficients from actual subjects, eight healthy adult volunteers (5 males and 2 females, age 19 to 35 years) who did not have contraindications to MR imaging were enrolled for scout scan imaging. A total of 60 ECG-gated, time-series 2-D coronal chest images were acquired per subject during free-breathing. Images were obtained during the measured cardiac rest period at end-diastole. All images were taken using steady-state free precession (SSFP) sequence in free breathing, acquired using a 1.5 T MRI scanner (Excelart Vantage, Toshiba Medical Systems, Tochigi, Japan). The study was approved by the Institutional Review Board of the Kyoto University Hospital and all subjects gave their informed written consent prior to enrolment in the study.

The reference scan used in the simulation was derived from a high-quality 3-D coronary MR angiography dataset [7]. The 3-D axial volume was acquired using SSFP sequence and consists of 140 slices acquired with TR = 4.3 ms, TE = 2.2 ms, slice thickness = 1.5 mm that was reconstructed as 0.75 mm thickness, acquisition matrix  $256 \times 168$  and reconstructed matrix size =  $512 \times 496$ . The dataset was cropped to remove the background and the neighbouring organs, resulting to a reduced matrix size of  $256 \times 168$ . The segmented heart serves as the reference image ( $Q_{Ref}$ ) for the respiration-induced deformation and respiratory gating simulation.

#### 3.1 Quantitative Image Quality Assessment

To validate the results of the simulations, an actual 3-D CMRA scan was acquired for the same volunteer whose motion coefficients were used for the simulation. This procedure allowed for the comparison of the simulated motion correction with that of an actual scan taken by the same volunteer. Five CMRA scans were acquired, one for each method described in Sect. 2.3.2. After the image acquisition, the 3-D images went through multiplanar reconstruc-

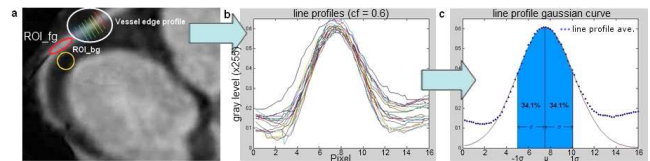


**Fig. 3** Curved MPR view of the right coronary artery near its origin in the aortic root (a). The regions of interests  $ROI_{fg}$  and  $ROI_{bg}$  are used for CNR calculations (b). The plot shows the multiple intensity line profiles (b), which are used to compute for sigma of the fitted Gaussian curve (c). The value of sigma is used to compute for the vessel edge definition.

tion to show the length of the coronary artery (Fig. 3). The same procedure was done for the simulated scans. The image quality of the simulated images were compared to that of the actual clinical scans to show the efficiency of the simulation system in evaluating the motion correction methods.

Quantitative image quality analysis were done using contrast-to-noise ratio (CNR) and vessel edge definition. The proximal and distal portion of the right coronary artery were selected as the regions of interest where these measures were applied. CNR is a well defined image quality measurement [8]–[10] and defined as the difference of signal intensities between the coronary artery and surrounding tissues divided by the background noise. Vessel edge definition, on the other hand, has been defined as how well the borders of a particular vessel are circumscribed [11]. Both of these measures determines the conspicuity of the coronary artery, which is important for an accurate diagnosis of clinically significant lesions.

Vessel edge definition is based on the calculation of signal gradients across the borders of the coronary artery. To measure its value, 20 line profiles are placed perpendicularly at the proximal part of the RCA (Fig. 3). The line profiles traverse both edges of the coronary artery, where the peak values correspond to the bright blood signal. Computation of the vessel edge definition here, however, is distinct from the one proposed by Dirksen et al [11]. Instead of using the down- and up-slope of the line profile set, a Gaussian curve was fitted into the average of the line profiles for edge calculation. The average value of all the curves was fitted with a Gaussian bell curve and the end variable that signifies the vessel edge definition was calculated as  $1/\sigma$ , where  $\sigma$  is the variance of the fitted curve. A smaller value of sigma corresponds to a steeper slope in the average signal intensity line profile, signifying a better vessel edge definition.

Finally, in order to statistically analyze the image quality between correction methods for the simulation and actual MR scan, the data has undergone a paired  $t$ -test analysis with a significance level of 0.05.

## 4. Results

The time-series coronal images acquired during the cardiac rest period under free-breathing enabled tracking of the upper and lower heart during respiration. There are wide variations in the measured  $CC$  values between subjects observed during the tracking of the scout scans. There was also a

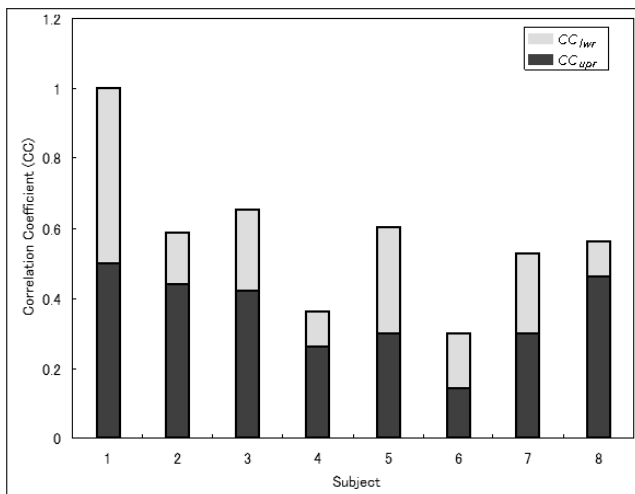


**Fig. 4** The measured correlation coefficient (CC) values for all the volunteer scans.  $CC_{upr}$  and  $CC_{lwr}$  indicates the translation of the upper and lower heart, respectively, for every 1 unit translation of the diaphragm. While  $CC_{mean}$  refers to the average of the two aforementioned values.

wide variation between the upper and lower heart motion. Lower heart correction factor ranges from 0.36 to 1.0, while upper heart has values of 0.14 to 0.53. Figure 4 shows the measured correlation coefficient values for all the scanned volunteers.

In the simulation experiments, image artifacts such as ghosting and image blurring occurred when data was acquired without motion correction. Consequently, significant reductions in motion artifacts were observed when the correction methods were employed. The simulation results also showed significant variations in image quality from the different motion compensation methods used.

#### 4.1 Coronary Artery Visualization

In Fig. 5, the proximal and distal cross-sections of the right coronary artery in show the effects of the different correction methods in the visual quality of the RCA. The figure shows the RCA cross-sections for both the simulated and clinical scans to validate the result of the simulations with that of an actual scan, with  $CC_{upr} = 0.46$  and  $CC_{lwr} = 0.56$ . The proximal cross-section was taken near the root of the RCA in the aorta while the distal cross-section was acquired from the main RCA vessel in the posterior region of the right ventricle. The columns (left to right) indicate the motion correction method used; namely, no motion correction,  $CF_{upr}$ ,  $CF_{mean}$ ,  $CF_{lwr}$ , and standard correction factor ( $CF = 0.6$ ).

The first column of Fig. 5 shows that the visibility of the coronary cross-section is almost zero if there is no correction used. The use of the upper heart correction factor ( $CF_{upr}$ ) results to a good vessel definition of the proximal RCA (Fig. 5 (G, Q)) but gives a barely visible distal cross-section (Fig. 5 (B, L)). On the other hand, employing the lower heart correction factor ( $CF_{lwr}$ ) gives a relatively better image quality in the distal part (Fig. 5 (D, N)) and but worse in the proximal cross-section (Fig. 5 (I, S)). The image qual-

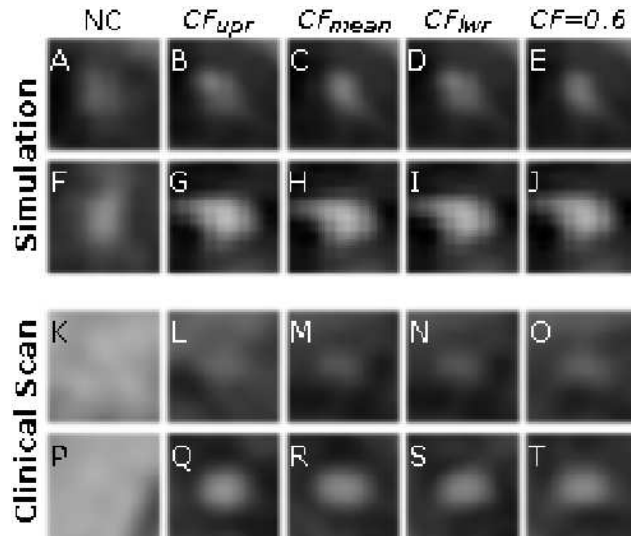


**Fig. 5** Shown are the cross-sections of the right coronary artery from the simulated (upper two rows) and clinical scans (bottom two rows). The first row of the simulated and clinical scan corresponds to the distal cross-section of the artery while the second row of each scan shows the proximal cross-section. The columns lists the motion correction methods used in the scans; namely, no motion correction (A, F, K, P),  $CF_{upr}$  (B, G, L, Q),  $CF_{mean}$  (C, H, M, R),  $CF_{lwr}$  (D, I, N, S), and standard correction factor (E, J, O, T).

ity of the coronary cross sections resulting from  $CF_{mean}$  is between that of the  $CF_{upr}$  and  $CF_{lwr}$ . Of the four correction factors used, the standard correction factor generally gives the worst image quality, especially with respect to the proximal RCA (Fig. 5 (J, T)). This is because its value is relatively far from the value of the actual  $CC_{upr}$  (0.46). The results also show that the relative effects of the different correction methods are consistent for both the simulation and actual clinical scan.

#### 4.2 Simulation vs. Reference Scan

In order to compare the effect of motion across one slice, the image differences between the middle coronal slice of the reference scan and the simulated scans for correlation coefficient pair of 0.5/1.0 ( $CC_{upr}/CC_{lwr}$ ) are shown in Fig. 6. It shows the effects of using different correction factors on the image quality at different areas of the heart. Compared with the reference image slice (Fig. 6 A), the image without motion correction (Fig. 6 B) experienced the most difference (*i.e.* image distortion). In Fig. 6 F, the bulk of the image difference and thus the residual motion artifact between the simulated slice and using the standard correction factor was highlighted. Since the correlation coefficient values used to transform these images are 0.5 and 1.0 for the upper and lower heart, respectively, the standard  $CF$  mostly corrected for motion in the upper heart since its value is closer to  $CC_{upr}$ . Using  $CF = CC_{lwr}$  results in residual motion artifacts around the upper region of the heart. In contrast, motion artifacts were not concentrated on any part of the heart when using the mean correction factor  $CF_{mean}$ . The mean

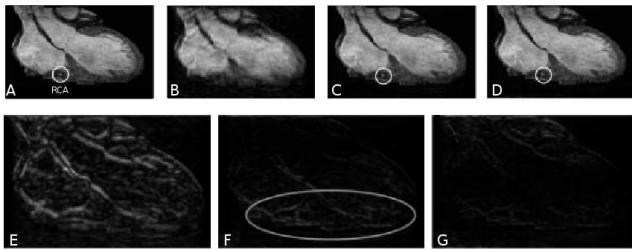


**Fig. 6** By getting the coronal slice of the 3-D image, the effect of respiratory motion on image quality and visibility of the distal RCA can be shown (top row). The middle coronal slice of the reference data (A) was compared with the simulated scans without motion correction (B), with  $CC_{upr}$  (C) and with  $CF_{mean}$  (D). The image difference between the reference slice and simulated slice without correction (E), with  $CC_{upr}$  (F) and with  $CF_{mean}$  (G) are also shown.

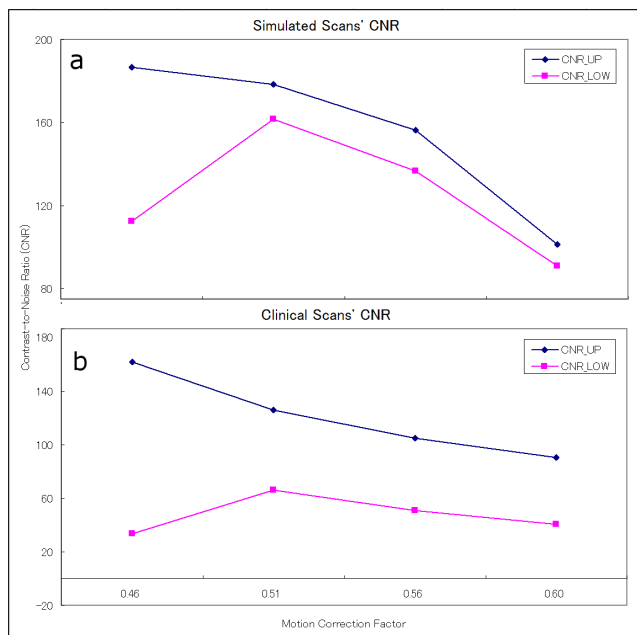


**Fig. 7** Contrast-to-noise ratio (CNR) measurements for the simulation and acquired clinical scans. The trend of the CNR measurements were consistent for both the simulation and actual scan. The scan acquired using the mean correction factor in average, gave the highest CNR while the standard correction factor gave the lowest.

correction factor gives the smallest difference from the reference image. This is confirmed by the results of the paired  $t$ -tests done between the results of using the mean correction factor and the other compensation methods, where the P value ranges from  $8.2 \times 10^{-7}$  (no correction) to  $4.0 \times 10^{-5}$  (using  $CF_{lwr}$ ).

### 4.3 Simulation vs. Clinical Scan

Validation of the simulation results was done by comparing the image quality of the simulated images with those of the actual clinical scans acquired using the same correction factors. Figure 7 shows the measured CNR values for the proximal (upper) and distal (lower) portions of the coro-

**Table 1** The average CNR values for the each correction factor used in the simulation and actual scans. The values for  $CF_{upr}$ ,  $CF_{mean}$  and  $CF_{lwr}$  are 0.46, 0.51 and 0.56, respectively.

Measure	Correction Factor			
	$CF_{upr}$	$CF_{mean}$	$CF_{lwr}$	0.6
Simulation	299.22	340.24	293.11	192.46
Clinical	191.22	191.86	155.80	130.90

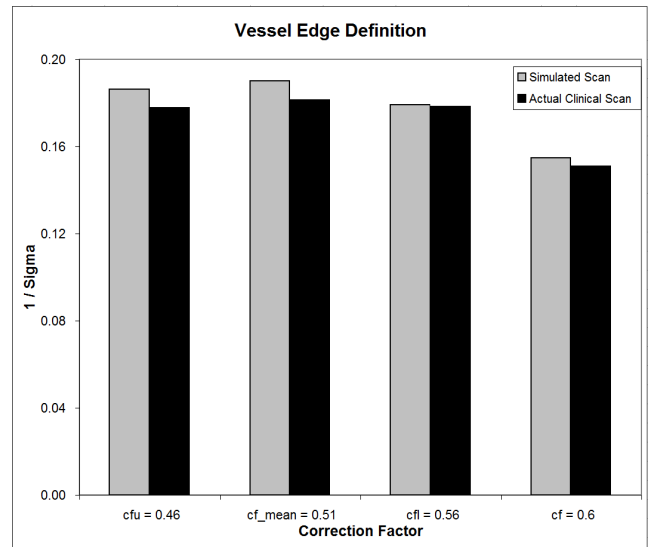


**Fig. 8** The vessel edge definition measurements for the simulation and actual clinical scans. The trends show a high correlation between the simulated and actual results ( $P = 0.038$ ).

nary artery for all the motion correction factors used. The measured upper and lower heart motion coefficient for the subject are 0.46 and 0.56, respectively. Results indicated that the proximal coronary artery image has a comparatively poor CNR when the lower heart correction factor is used and vice versa. The factor  $CF_{mean}$ , on average, gave the best CNR for all the factors used while the use of the standard correction factor (0.6) gave the worst. This trend is consistent for both the simulation and the actual scans as shown in Fig. 7 b. Table 1 summarizes the mean CNR values for the four different correction methods used. Acquisitions using the mean correction factor showed the highest CNR for both the simulation (340.22) and the actual scan (191.86).

The same observation is applicable to the results of the vessel edge definition measurements (Fig. 8). The trend in the simulation scan showed high correlation with that of the clinical scans ( $P = 0.038$ ).

## 5. Discussion

A critical aspect of choosing a respiratory motion correction method is its impact on the resulting MR image quality. This is evident especially in the case of coronary imaging like CMRA where a small difference in the respiratory gating can have adverse effects in the detection of lesions or blockages. However, the comparative effectiveness of the available correction methods is difficult to evaluate using

actual MR scans. This is due to the difficulty in obtaining a ground truth, an assessment not effected by other sources of artifacts like cardiac cycle or magnetic field noise. Thus, we proposed an alternative, to use simulation as a tool and realistically recreate the data acquisition process during an MRI scan. The results of the experiments demonstrated that the simulation platform can be used to induce respiratory motion in the image and simulate the application of different motion correction methods.

The image-quality measures showed the effects on image quality of the respiratory motion correction factors used. These factors are translation coefficients simulating the use of the subject-specific navigator-guided techniques, which are prevalent in clinical CMRA scans. If the SI motion of the heart due to diaphragm motion is significantly less than 0.6, using the standard correction factor overestimates the motion, thus increasing the induced motion and decreasing image quality. This poses a significant drawback of using the same correction factor for all patients since in cases of minimal respiratory motion, it adds rather than correct motion. Additionally, the increase from the uncorrected data in terms of SNR ( $P = 0.0091$ ), CNR ( $P = 0.0009$ ) and vessel edge definition ( $P = 0.0087$ ) is highest when using the mean correction factor.

Aside from the dominant SI motion during respiration, displacement in other directions was also observed. However, the measured values from the volunteer scans were very small compared to SI motion. The measured right-left (RL)  $CC$  also have low correlation with diaphragm motion (average  $R^2 < 0.4$ ). This may be due to the fact that our tracking method is not robust enough to locate the specific ROI edge as it moves in the SI direction. Unlike the case for the tracking the horizontal edge in the SI direction, tracking the vertical edge as it moves in the RL direction presents more challenges because of the dominant SI movement. We plan to improve on the robustness of our tracking method in order to provide a more accurate estimation of correlation coefficients.

Using the platform for CMRA scans with the prospective 1-D respiratory motion correction method may help in improving output image quality. A clinician can test different  $CF$  values in the simulator and determine which one would be the most suitable for a certain subject or patient. This subject-specific  $CF$  can then be used to replace the standard correction factor to acquire a better-quality CMRA image.

The current modelling of respiratory motion involves the tracking of 2-D motion only. Tracking the 3-D motion is also possible although it would present challenges because two planes has to be tracked (coronal and sagittal). The 3-D compensation may also be impractical to implement in most scanners.

The hardware capability of MR scanners is still one of the main restrictions in the implementation of respiratory correction methods. Different models from different manufacturers offer varying technical challenges in addressing motion artifacts from respiration. For this reason, self-

gating methods using image-based tracking are gaining acceptance since it can be applied to most MR scanners without significant hardware changes. Future work will include the evaluation of these self-gating approaches and also further validation using additional clinical MR scans.

## 6. Conclusion

This study demonstrated an overview of a simulation platform for MR respiratory motion correction. The model can be used to evaluate different motion correction techniques without the need to perform actual scans, which are subject to other sources of image artifacts aside from respiratory motion. The results of the simulation experiments showed high correlation with those of the actual scan. This reflects the capability of the simulation platform to recreate the effects of respiratory motion in CMRA scans. The system also allows the flexibility to test different parameter estimation algorithms and MR  $k$ -space image reconstruction methods.

Although the simulator functions well in its current state, several issues remain to be addressed. Additional parameter estimation and more advanced  $k$ -space reconstruction techniques would be useful. Furthermore, there are many possible improvements that could help improve the overall realism of the output. With more features, we are confident that this simulator can be modified to evaluate a wide variety of cardiac motion correction algorithms.

## Acknowledgments

The authors would like to thank Kei Wai Cecilia Hung and Raula Kula for the proofreading and support, the people of Toshiba MR Systems Division for their assistance and MPR software, and those who volunteered for the MR scout scans.

## References

- [1] E.A. Zerhouni, D.M. Parish, W.J. Rogers, A. Yang, and E.P. Shapiro, "Human heart: Tagging with MR imaging—a method for noninvasive assessment of myocardial motion," *Radiology*, vol.169, pp.59–63, 1988.
- [2] A.M. Taylor, J. Keegan, P. Jhooti, D.N. Firmin, and D.J. Pennell, "Calculation of a subject-specific adaptive motion-correction factor for improved real-time navigator echo-gated magnetic resonance coronary angiography," *J Cardiovasc Magn Reson*, vol.1, pp.131–138, 1999.
- [3] R.W. Fischer, R.M. Botnar, K. Nehrke, P. Boesiger, W.J. Manning, and D.C. Peters, "Analysis of residual coronary artery motion for breath hold and navigator approaches using real-time coronary MRI," *Magn Reson Med*, vol.55, pp.612–618, 2006.
- [4] K. Nehrke and P. Bornert, "Prospective correction of affine motion for arbitrary MR sequences on a clinical scanner," *Magn Reson Med*, vol.54, pp.1130–1138, Nov. 2005.
- [5] D. Manke, K. Nehrke, P. Bornert, P. Rosch, and O. Dossel, "Respiratory motion in coronary magnetic resonance angiography: A comparison of different motion models," *J Magn Reson Imaging*, vol.15, pp.661–671, 2002.
- [6] S.D. Roes, G. Korosoglou, M. Schar, J.J. Westenberg, M.J. van Osch, A. de Roos, and M. Stuber, "Correction for heart rate variability during 3D whole heart MR coronary angiography," *J Magn Reson Imaging*, vol.27, pp.1046–1053, 2008.

- [7] T. Okada, S. Kanao, A. Ninomiya, S. Sato, S. Kuhara, T. Kamae, K. Gotoh, and K. Togashi, "Whole-heart coronary magnetic resonance angiography with parallel imaging: Comparison of acceleration in one-dimension vs. two-dimensions," *Eur J Radiol*, vol.71, pp.486–491, Sept. 2009.
- [8] R.M. Botnar, M. Stuber, P.G. Danias, K.V. Kissinger, and W.J. Manning, "Improved coronary artery definition with T2-weighted, free-breathing, three-dimensional coronary MRA," *Circulation*, vol.99, pp.3139–3148, June 1999.
- [9] D. Li, J. Zheng, and H.J. Weinmann, "Contrast-enhanced MR imaging of coronary arteries: comparison of intra- and extravascular contrast agents in swine," *Radiology*, vol.218, pp.670–678, March 2001.
- [10] M.B. Hofman, R.E. Henson, S.J. Kovacs, S.E. Fischer, R.B. Lauffer, K. Adzamlı, J. De Becker, S.A. Wickline, and C.H. Lorenz, "Blood pool agent strongly improves 3D magnetic resonance coronary angiography using an inversion pre-pulse," *Magn Reson Med*, vol.41, pp.360–367, Feb. 1999.
- [11] M.S. Dirksen, H.J. Lamb, R. van der Geest, and A. de Roos, "Toward comparability of coronary magnetic resonance angiography: Proposal for a standardized quantitative assessment," *Eur Radiol*, vol.13, pp.2353–2357, Oct. 2003.



**Shigehide Kuhara** graduated from the Department of Information Engineering in Kyushu University in 1983 and his Ph.D. at the same university in 2010. He joined the Toshiba R&D Center at Kawasaki. He is involved in MRI systems development, especially in ultra fast MRI (EPI) systems. He currently belongs to the MRI Systems Group, MRI Development Department, MRI Systems Division of Toshiba. He is mainly in charge of developing technology for cardiac MRI and its applications.



**Kaori Togashi** received her Ph.D. degree at Kyoto University Graduate School of Medicine in 1987. She worked as an assistant and associate professor, and in 2004, became a professor and chairperson of Kyoto University Graduate School of Medicine (Diagnostic Imaging and Nuclear Medicine). She belongs to the following societies as committee member: International Society of Magnetic Resonance in Medicine, Japanese Society of Magnetic Resonance in Medicine, Japanese Radiological Society, and others.

ety, and others.



**Florencio Rusty Punzalan** received his Master of Science degree in Electronics Engineering from Ateneo de Manila University, Philippines in 2008. He is currently pursuing his Ph.D. in Biomedical Imaging and Informatics Lab. in Nara Institute of Science and Technology. He is also currently working as a Researcher in the Biosimulation Lab. in Ritsumeikan University. His research interests include cardiac imaging and simulation.



**Kotaro Minato** received his M.S. and Ph.D. degrees in Electrical Engineering from Kyoto University, Kyoto, Japan, in 1972 and 1980, respectively. He is currently the professor in Biomedical Imaging and Informatics Laboratory and Dean of the School of Information Science in Nara Institute of Science and Technology. His research interests include medical imaging, biomedical engineering and medical informatics.



**Tetsuo Sato** received his Ph.D. degree in engineering from Nara Institute of Science and Technology in 2001. He was a research fellow of Fukui Medical University (2001–2002) and Japan Science and Technology Agency (2002–2003). He is an assistant professor at Nara Institute of Science and Technology since 2003. His current research interests are medical image processing and biomedical engineering.



**Tomohisa Okada** graduated from Kyoto University Medical School in 1990. He took 5 years of residency in Tenri Yorodu Hospital. Thereafter, he got his Ph.D. degree at Kyoto University Graduate School of Medicine and became an assistant professor at National Institute of Physiological Sciences at Okazaki. He also worked at the Institute of Biomedical Research and Innovation of Kobe City General Hospital. He is currently working in Kyoto University Hospital as a lecturer for MRI, PET and SPECT examinations, mainly in brain imaging. He is a member of JAMIT, Japan Society of Magnetic Resonance in Medicine, and Japan Radiological Society.